## Supporting Information

# Reversibly metal-induced emission and chromaticity switching in isostructural Ln-MOFs

Yue Tong, Xiao Han, Chao Huang, Zhichao Shao, Li'an Guo, Yazhen Wang, Jie Ding* and Hongwei Hou*

The college of Chemistry and Molecular Engineering, Zhengzhou University, Zhengzhou, Henan, 450001, P. R. China.

Email: jieding@zzu.edu.cn

Email: houhongw@zzu.edu.cn

**Materials and physical measurements:** All reagents and solvents were commercially available and were used without further purification. The FT-IR spectra of samples in dry KBr disks were recorded in the range of 400-4000 cm$^{-1}$ on Bruker Tensor 27 spectrophotometer. Elemental analyses (C, N and H) were carride out on a FLASH EA 1112 elemental analyzer. PXRD patterns were performed using Cu K$\alpha_1$ radiation on a PANalytical X'Pert PRO diffractometer in room-temperature. Thermal analyses (TGA) were obtained on a Netzsch STA 449C thermal analyzer from room temperature at a heating rate of 10 °C min$^{-1}$ in air. The emission studies of the powdered solid samples were conducted on a Hitachi 850 fluorescence spectrophotometer at ambient temperature. Inductively coupled plasma spectra (ICP) were performed on a Thermo ICAP 6500 DUO spectrometer. The Commission International de I'Eclairage (CIE) color cooradinates were calculated on the basis of the international CIE standards. The surface morphologies and energy dispersive X-ray spectra of samples were measured by a field-emission scanning electron microscopy (FE-SEM, JEOL-JSM-6700F, Japan) equipped with an energy dispersive X-ray spectroscopy (EDS) system.

**Synthesis of complexes 1-3:** *A mixture of* $Ln(NO_3)_3{\cdot}6H_2O$ *(0.1 mmol) (Ln = Tb (**1**), Gd (**2**), Eu (**3**)), pyridine-3,5-bis(phenyl-3-carboxylic acid)(*$H_2L$*, 0.0192 g, 0.06 mmol), N, N-Dimethylacetamide (DMAC, 4 mL),* $HNO_3$ *(14 mol/L, 4 drops),* $H_2O$ *(2 mL) was sequentially added in a Teflon-lined reactor and sealed at 120 °C for 3 days. After being cooled to room temperature, the cubic crystals were obtained by filtration, and washed with DMAC and* $H_2O$*. Yield: about 70% based on Ln(III). For **1**: C, 50.87; N, 3.71; H, 3.13 %. Found: C, 50.80; N, 3.79; H, 3.14 %. Selected IR (KBr pellet, v/cm*$^{-1}$*): 3410(s), 3063(m), 2171(m), 1604(vs), 1552(vs), 1430(vs), 1393(vs), 1273(m), 1134(s), 894(m), 767(s), 570(m). For **2**: C, 51.06; N, 3.72; H, 3.14 %. Found: C, 51.16; N, 3.80; H, 3.10 %. Selected IR (KBr pellet, v/cm*$^{-1}$*): 3423(s), 3063(m), 2171(m), 1606(vs), 1552(vs), 1431(vs), 1394(vs), 1274(m), 1128(s), 896(m), 767(s), 566(m). Crystal data: a = 13.437(3) Å, b = 15.526(3) Å, c = 18.319(4) Å.* $\alpha = 90$, $\beta = 103.17(3)$, $\gamma = 90°$*. For **3**: C, 51.47; N, 3.75; H, 3.16 %. Found: C, 50.84; N, 3.82; H, 3.14 %. Selected IR (KBr pellet, v/cm*$^{-1}$*): 3419(s), 3063(m), 2171(m), 1605(vs), 1548(vs), 1430(vs), 1391(vs), 1273(m), 1129(s), 895(m), 767(s), 563(m). Crystal data: a = 13.6762(143) Å, b = 15.5840(152) Å, c = 18.6757(188) Å.* $\alpha = 90$, $\beta = 103.5415(112)$, $\gamma = 90°$*.*

**Synthesis of** $\mathbf{Gd_{0.81}Tb_{0.10}Eu_{0.09}L}$ **doped complex 4***: A mixture of* $Gd(NO_3)_3{\cdot}6H_2O$ *(0.0361 g, 0.08 mmol),* $Tb(NO_3)_3{\cdot}6H_2O$ *(0.0045 g, 0.01 mmol),* $Eu(NO_3)_3{\cdot}5H_2O$ *(0.0043 g, 0.01 mmol), pyridine-3,5-bis(phenyl-3-carboxylic acid)(*$H_2L$*, 0.0192 g, 0.06 mmol), N, N-Dimethylacetamide (DMAC, 4 mL),* $HNO_3$ *(14 mol/L, 4 drops),* $H_2O$ *(2 mL) was sequentially added in a Teflon-lined reactor and sealed at 120 °C for 3 days. After being cooled to room temperature, the cubic crystals were obtained by filtration, and washed with DMAC and* $H_2O$*. Yield: about 72% based on Ln(III). C, 51.09; N, 3.73; H, 3.09 %. Found: C, 51.36; N, 3.74; H, 3.17 %. ICP: Gd, 81.25; Tb, 9.54; Eu, 9.21 %. Selected IR (KBr pellet, v/cm*$^{-1}$*): 3404(s), 3063(m), 2171(m), 1605(vs), 1551(vs), 1430(vs), 1391(vs), 1273(m), 1134(s), 895(m), 767(s), 570(m).*

**Synthesis of** $\mathbf{Gd_{0.75}Tb_{0.18}Eu_{0.07}L}$ **doped complex 5***: A mixture of* $Gd(NO_3)_3{\cdot}6H_2O$ *(0.0338 g, 0.075 mmol),* $Tb(NO_3)_3{\cdot}6H_2O$ *(0.0082 g, 0.018 mmol),* $Eu(NO_3)_3{\cdot}5H_2O$ *(0.0030 g, 0.007 mmol), pyridine-3,5-bis(phenyl-3-carboxylic acid)(*$H_2L$*, 0.0192 g, 0.06 mmol), N, N-Dimethylacetamide (DMAC, 4 mL),* $HNO_3$ *(14 mol/L, 4 drops),* $H_2O$ *(2 mL) was sequentially added in a Teflon-lined reactor and sealed at 120 °C for 3 days. After being cooled to room temperature, the cubic crystals were obtained by filtration, and washed with DMAC and* $H_2O$*. Yield: about 73% based on Ln(III). C, 51.08; N, 3.72; H, 3.09 %. Found: C, 51.57; N, 3.73; H, 3.14 %. ICP: Gd, 75.14; Tb, 17.49; Eu, 7.37 %. Selected IR (KBr pellet, v/cm*$^{-1}$*): 3413(s), 3063(m), 2171(m), 1605(vs), 1549(vs), 1431(vs), 1391(vs), 1274(m), 1131(s), 895(m), 767(s), 568(m).*

**X-ray crystal structure determination:** The data for MOF **1** was collected on a SuperNova Single Crystal Diffractomer (Cu-Kα, λ = 1.5418 Å) at a temperature of 20 ± 1 °C. Absorption corrections were applied by using a multi-scan program. The data were corrected for Lorentz and polarization effects. The structures were solved by direct methods and refined with a full-matrix least-squares technique based on $F^2$ with the SHELXL-97 crystallographic software package. The ligand and Tb2 is disorder over at least two major positions with approximate 2:1 occupancy ratio. The disorder is most likely continuous so in order to better describe the structure most of the displaced parameters have been refined anisotropically and with DELU/SIMU restraints. ISOR instructions in SHELXL were imposed on C13A, C13B, C14A, C14B, C15A, C15B, N2A, N2B, C17A, C17B, C18A, C18B, C19A, C19B, C20A, C20B, C21A, C21B, C22A, C22B, C5A, C5B, C6A, C6B, C7A, C7B, O1A, O1B, O2A, O2B, O5A, O5B, O7A, O7B, O3A, O3B, Tb2A, and Tb2B atoms to get reasonable displacement parameters. The contribution of solvent molecules was treated as diffuse using SQUEEZE procedure implemented in the PLATON program.[1] The numbers of solvent molecules were obtained by elemental analyses and TGA. Crystallographic crystal data and structure processing parameters for **1** are summarized in Table S1 (ESI†). Selected bond lengths and bond angles of **1** are listed in Table S2 (ESI†).

**The detail single-crystal structure description of complex 1 and the thermal stability of complexes 1-5:** The crystal of sample **1** belongs to the monoclinic system with space group *$P2_1/c$*, indicating a noninterpenetrated windmill-shaped 3D framework (Fig. S2, ESI†). As shown in Figure S2a, the asymmetric unit was constructed by two independent $Tb^{3+}$ ions, two $L^{2-}$, two coordinated water molecules and one coordinated $OH^-$. Herein, Tb1 ion was coordinated by six O atoms (O1A, O6, O7A, O8, O9#A, 010#B) from carboxylate groups of ligands, one O (O4) atom from $OH^-$ and one N (N7) atom from $L^{2-}$, resulting in a distorted bicapped-triprismatic coordination geometry. On the other hand, for Tb2 ion, it was coordinated with four O atoms (O2A, O2A#C, O5A, O5A#C) from $L^{2-}$, two O atoms (O4, O4#C) from $OH^-$ and two O atoms (O3A, O3A#C) from water molecules. The Tb-O bond lengths were in the range of 2.279(6)-2.902(12) Å and the length of Tb-N was 2.610(6) Å. The $L^{2-}$ in **1** were completely deprotonated, and adopted two different coordination modes, respectively. The first type of $L^{2-}$ acted as a penta-connector to link five Tb atoms with the participation of N atom (Mode 1 of Scheme 1, ESI†), whereas the second type of $L^{2-}$ adopted $((\kappa_1\text{–}\kappa_1)\text{–}\mu_2)\text{-}(\kappa_1\text{-}\kappa_1\text{-}\mu_2)\text{-}\mu_4$ coordination mode connecting four Tb atoms (Mode 2 of Scheme 1, ESI†) with an uncoordinated N atom. On the basis of these connection modes, Tb1 and Tb2 atom were linked together by two carboxylate groups and one $OH^-$ in a $\kappa_1\text{-}\kappa_1\text{-}\mu_2$ style to give a binuclear unit. Furthermore, the binuclear units and adjacent Tb1 were connected commutatively adopting the coordination Mode 2 by the carboxylate bridges to assemble into a 2D wavelike layer. At last, such layers interconnected in a parallel manner were united each other via the coordination Mode 1 to afford a 3D framework. Although this kind of Ln-MOF showed the irregular cavity, the solvent-accessible volume from the crystal structure was estimated by PLATON to only be 6.9% of the total volume. Moreover, TGA experiment was performed under air atmosphere to check the thermal stability of MOF **1**-**5**. As shown in Fig. S3, the thermogravimetric images of MOF **1**-**5** are very similar, so only the complex **1** will be discussed in the range of 20-800 °C. For instance, the first weight loss of 7.59% (calcd 7.47%) was successively observed in the range of 0-397 °C, attributing to the loss of the solvent molecules. Subsequently, from 400 °C to 500 °C, a less than 5% loss gradually observed was indicating the startlingly decomposition of this sample. When the temperature was over 500 °C, the decomposition process was suddenly accelerated, suggesting the full collapse of the backbone in sample **1**. The total weight loss of 62.52% (calcd 63.38%) was in the range of 398-604 °C, and the final residues were the deposition of the corresponding oxides.

**Table S1.** Crystal data and structure refinement for complex **1**.

| Complex | 1 |
|---|---|
| formula | $C_{80}H_{58}N_5O_{20}Tb_3$ |
| fw | 1886.07 |
| T/K | 293(2) K |
| λ (Cu K), Å | 1.5418 Å |
| Cryst syst | Monoclinic |
| Space group | *P2₁/c* |
| a (Å) | 13.3571(2) Å |
| b (Å) | 15.1847(2) Å |
| c (Å) | 18.2750(3) Å |
| α (°) | 90 |
| β (°) | 103.6320(10) |
| γ (°) | 90 |
| V (Å$^3$) | 3602.18(9) |
| Z | 2 |
| $D_{calcd}$.(gcm$^{-3}$) | 1.659 |
| abs coeff/mm$^{-1}$ | 14.848 mm$^{-1}$ |
| F(000) | 1760 |
| θ (°) | 3.83-76.48 |
| GOF | 1.042 |
| $R_1$(I>2sigma(I))[a] | 0.0773 |
| $wR_2$(I>2sigma(I))[b] | 0.2039 |

[a] $R_1 = \Sigma\|F_o| - |F_c\|/\Sigma|F_o|$ and [b] $wR_2 = \{\Sigma[w(F_o^2 - F_c^2)^2]/\Sigma[w(F_o^2)^2]\}^{1/2}$.

**Table S2.** Selected bond lengths [Å] and angles [°] for complex **1**.

| MOF **1** | | | |
|---|---|---|---|
| Tb(1)-O(8) | 2.279(6) | Tb(1)-O(4) | 2.507(13) |
| Tb(1)-O(6) | 2.312(6) | Tb(1)-N(7) | 2.610(6) |
| Tb(1)-O(7A) | 2.314(15) | Tb(2A)-Tb(2A)#8 | 1.125(4) |
| Tb(1)-O(9)#1 | 2.314(5) | Tb(2A)-O(5A) | 2.095(11) |
| Tb(1)-O(1A) | 2.328(10) | Tb(2A)-O(2A) | 2.268(10) |
| Tb(1)-O(10)#2 | 2.349(5) | Tb(2A)-O(5A)#8 | 2.902(12) |
| | | | |
| O(8)-Tb(1)-O(6) | 81.4(3) | O(9)#1-Tb(1)-O(4) | 140.1(4) |
| O(8)-Tb(1)-O(7A) | 124.7(4) | O(1A)-Tb(1)-O(4) | 65.8(5) |
| O(6)-Tb(1)-O(7A) | 136.6(4) | O(10)#2-Tb(1)-O(4) | 73.0(4) |
| O(8)-Tb(1)-O(9)#1 | 78.1(3) | O(8)-Tb(1)-N(7) | 76.7(2) |
| O(6)-Tb(1)-O(9)#1 | 144.4(2) | O(6)-Tb(1)-N(7) | 72.3(2) |
| O(7A)-Tb(1)-O(9)#1 | 78.8(4) | O(7A)-Tb(1)-N(7) | 141.2(4) |
| O(8)-Tb(1)-O(1A) | 148.7(3) | O(9)#1-Tb(1)-N(7) | 74.80(19) |
| O(6)-Tb(1)-O(1A) | 100.6(3) | O(1A)-Tb(1)-N(7) | 74.3(3) |
| O(7A)-Tb(1)-O(1A) | 74.7(5) | O(10)#2-Tb(1)-N(7) | 140.7(2) |
| O(9)#1-Tb(1)-O(1A) | 83.1(3) | O(4)-Tb(1)-N(7) | 116.5(4) |
| O(8)-Tb(1)-O(10)#2 | 74.9(2) | O(5A)-Tb(2A)-O(2A) | 93.2(4) |
| O(6)-Tb(1)-O(10)#2 | 77.1(2) | Tb(2A)#8-Tb(2A)-O(3A) | 120.9(4) |
| O(7A)-Tb(1)-O(10)#2 | 77.9(4) | O(5A)-Tb(2A)-O(3A) | 81.7(5) |
| O(9)#1-Tb(1)-O(10)#2 | 124.0(2) | O(2A)-Tb(2A)-O(3A) | 82.6(5) |
| O(1A)-Tb(1)-O(10)#2 | 136.2(3) | Tb(2A)#8-Tb(2A)-O(5A)#8 | 35.7(2) |
| O(8)-Tb(1)-O(4) | 140.3(4) | O(5A)-Tb(2A)-O(5A)#8 | 161.71(14) |
| O(6)-Tb(1)-O(4) | 69.3(4) | O(2A)-Tb(2A)-O(5A)#8 | 103.4(3) |
| O(7A)-Tb(1)-O(4) | 69.7(5) | O(3A)-Tb(2A)-O(5A)#8 | 107.7(4) |

Symmetry codes: #1 -x+1,y-1/2,-z+1/2; #2 x,-y+1/2,z-1/2; #8 -x+2,-y,-z.

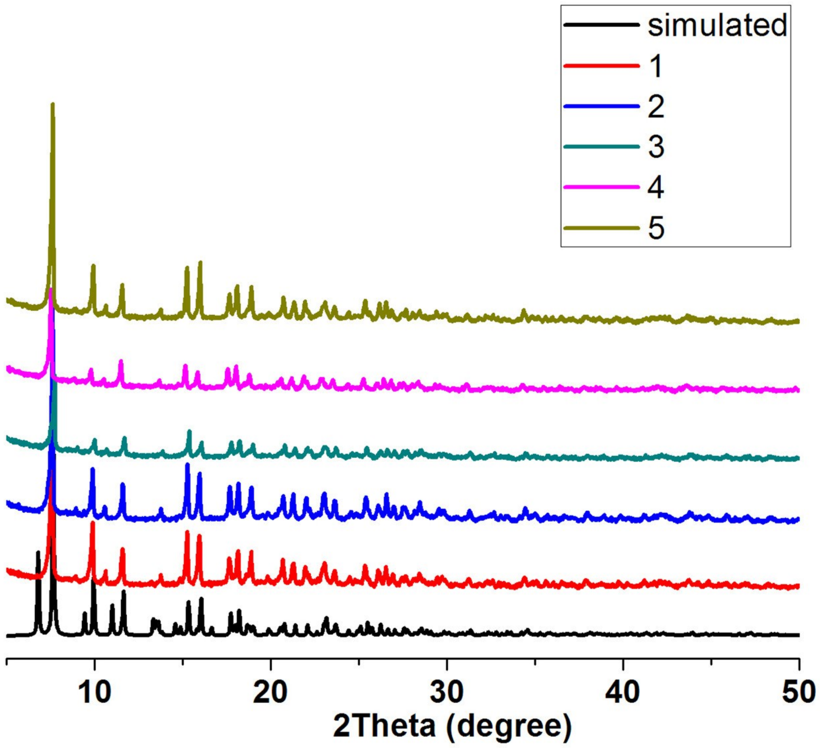

**Figure S1.** Powder XRD patterns of complexes **1-5** in the range from 5 to 50 degrees. (When θ = 6.8 degree, the peak corresponding to (1, 0, 0) was absent in the experimental pattern.)

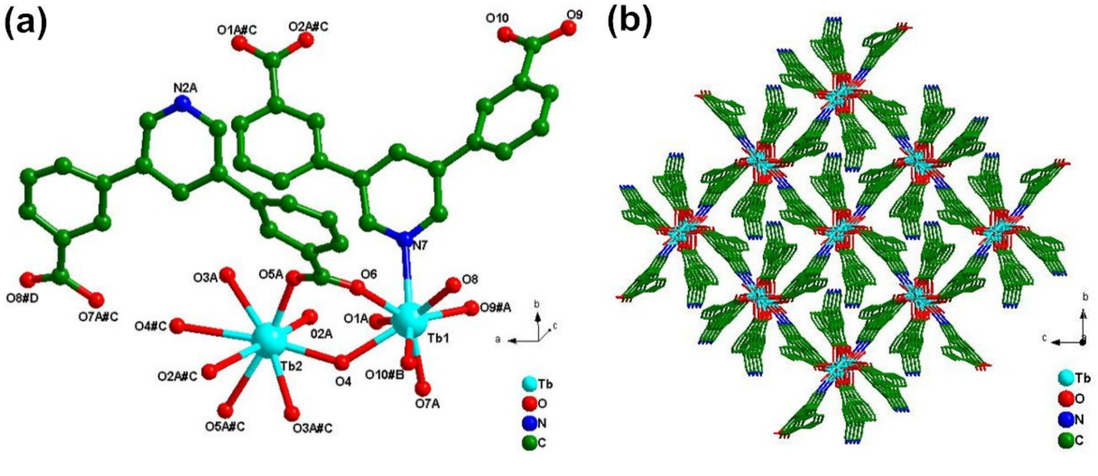

**Figure S2.** (a) Coordination environment around Tb(III) in MOF **1**, H atoms and lattice solvent molecules are omitted for clarity (Tb, cyan; O, red; N, blue; C, green). Symmetry codes: #A -x+1, y-1/2, -z+1/2; #B x, -y+1/2, z-1/2; #C -x+2, -y, -z; #D x+1, y, z; (b) 3D crystal structure of **1**, 3D crystal structure of **1**, hydrogen atoms and lattice solvent molecules are omitted for clarity.

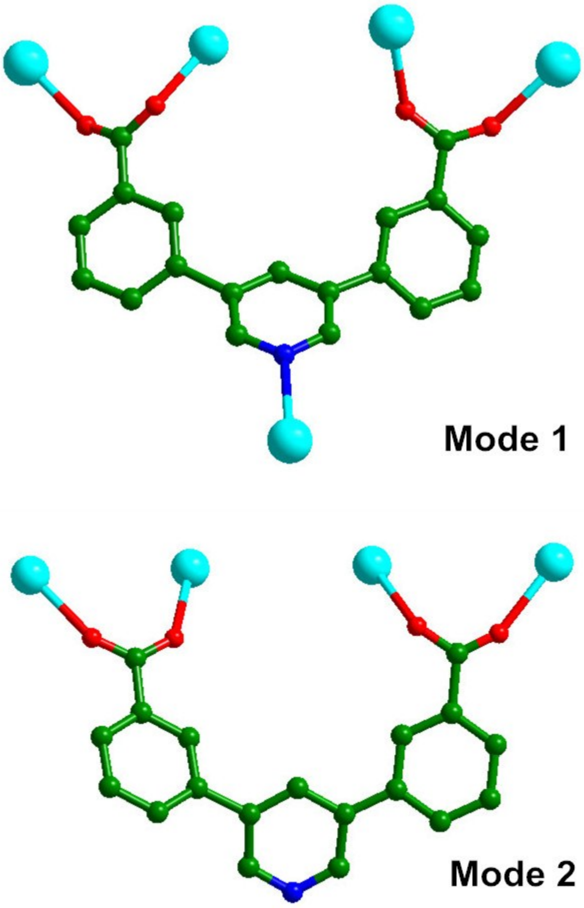

**Scheme 1.** Coordination mode of ligand $H_2L$ in **1**.

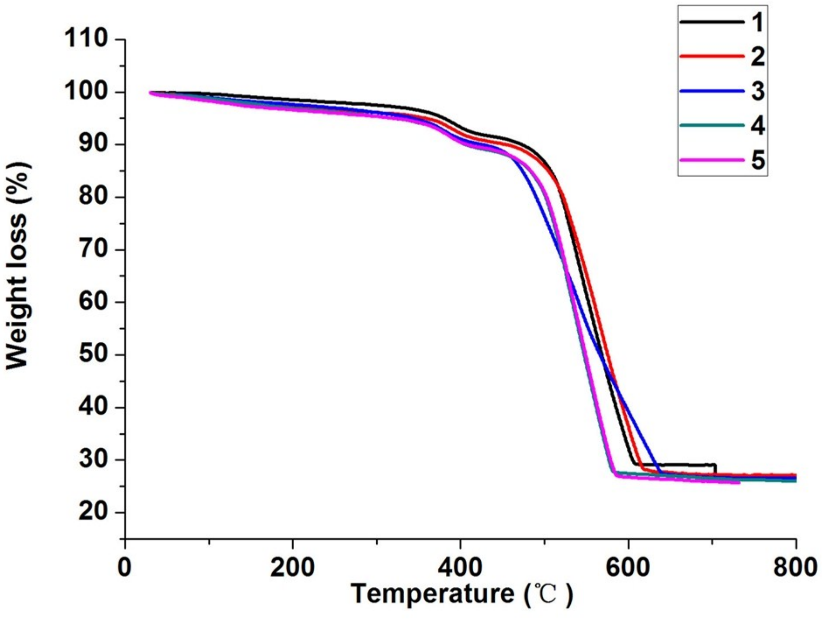

**Figure S3.** Thermogravimetric analyses (TGA) curve of complexes **1-5**.

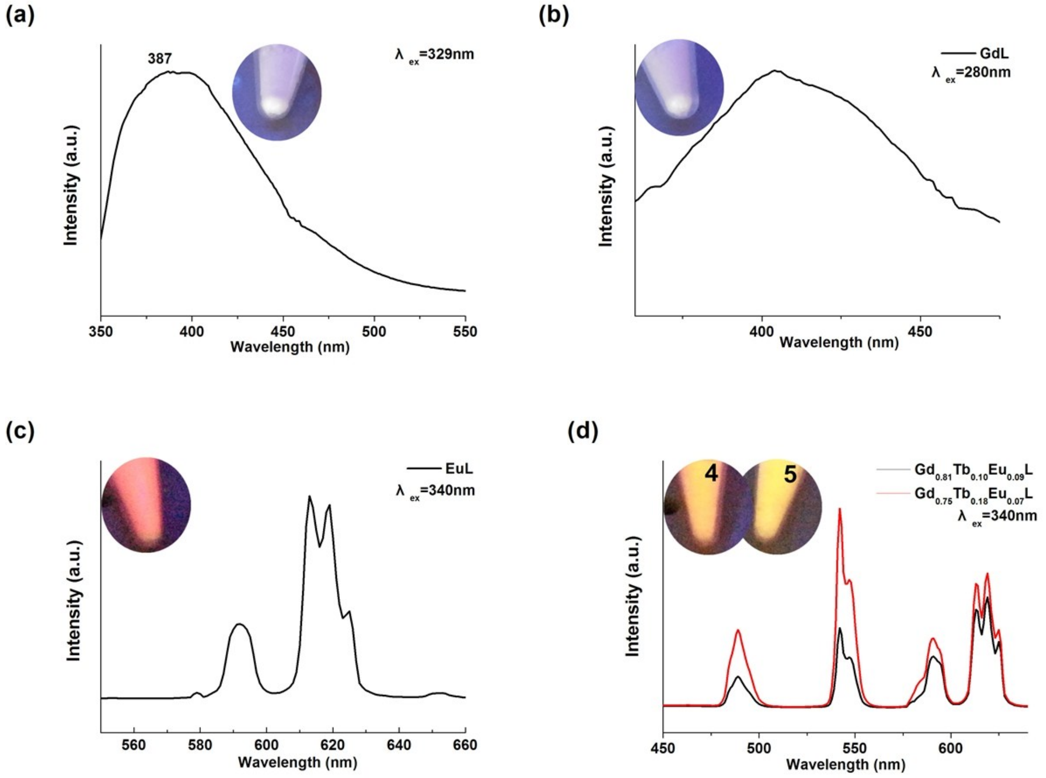

**Figure S4.** The emission spectra of the solid-state complexes: (a) $H_2L$ ligand; (b) **2**; (c) **3**; (d) **4** and **5**; (inset) the image of corresponding compound under the irradiation of 265 nm UV light.

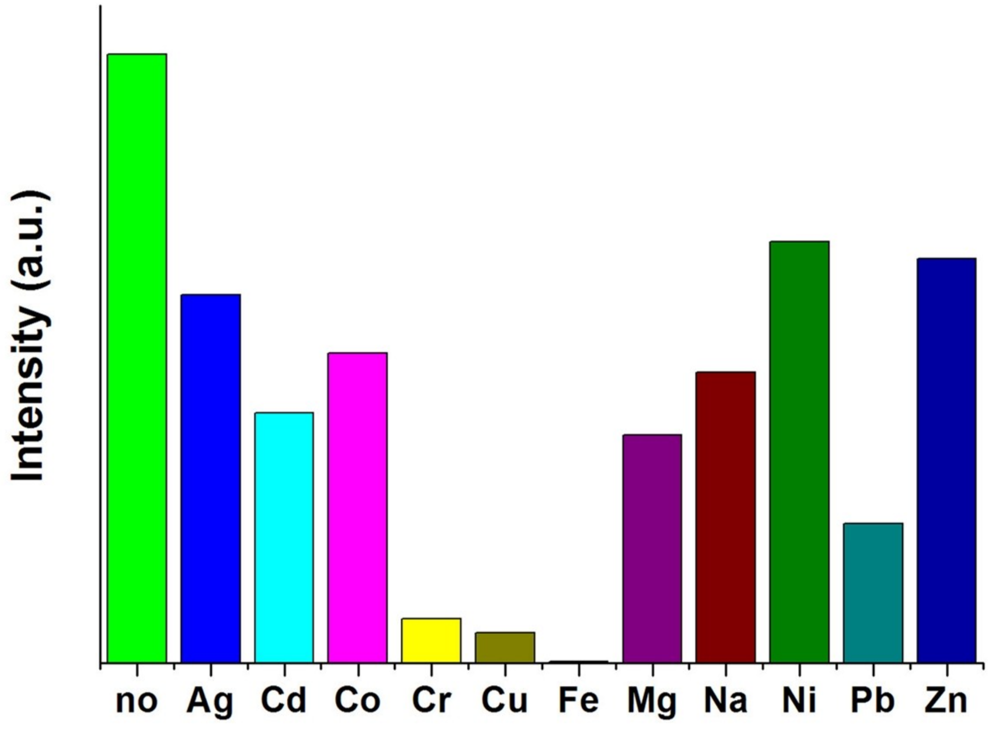

**Figure S5.** Comparison of the luminescence intensity of $M^{n+}$-**1** in $10^{-2}$ M different metal ions at 543 nm.

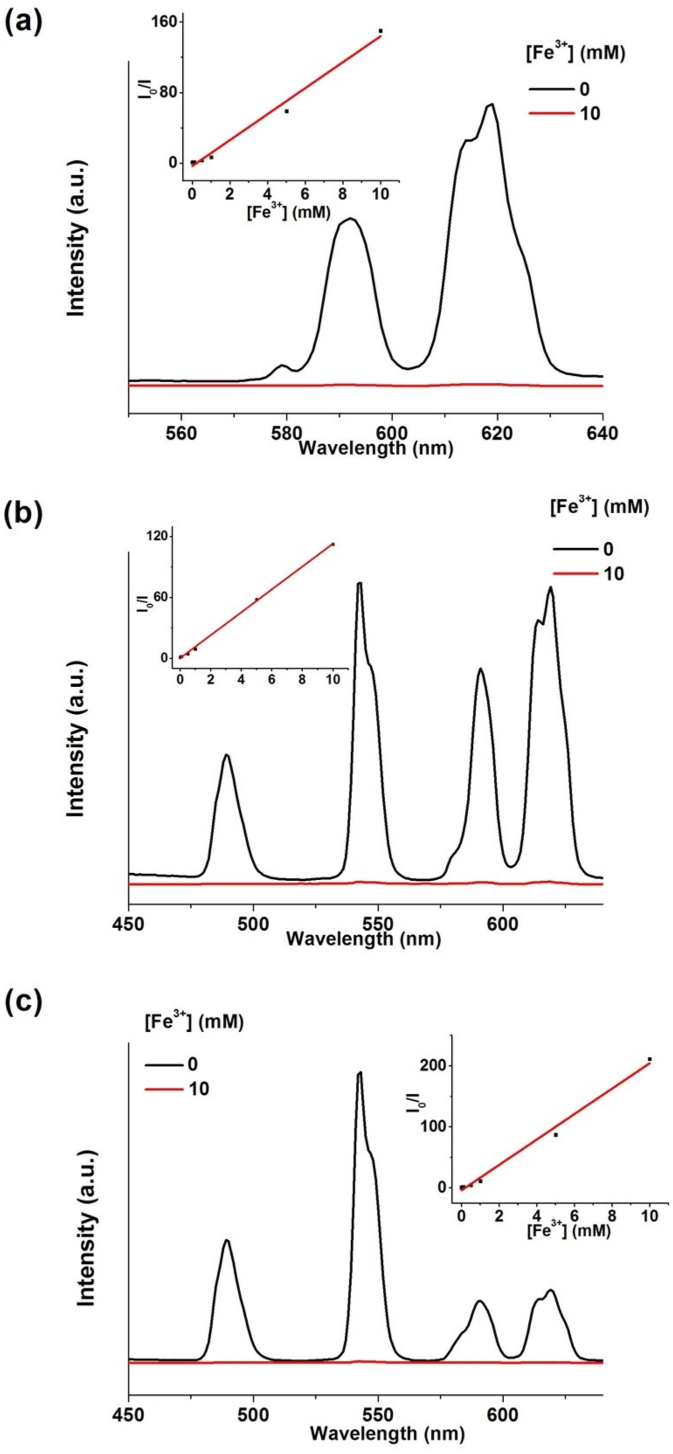

**Figure S6.** (a) The luminescence intensity of complex **3** upon addition of different concentrations of $Fe(NO_3)_3$ ethanol solutions, (inset) the dose-response graph at 619 nm revealing the Stern−Volmer quenching constant $K_{SV}$ was 0.0015 $\mu M^{-1}$ ($r^2$=0.986); (b) the luminescence intensity of complex **4** in different concentrations of $Fe(NO_3)_3$ ethanol solutions, (inset) the dose-response graph at 543 nm revealing the Stern−Volmer quenching constant $K_{SV}$ was 0.0011 $\mu M^{-1}$ ($r^2$=0.998); (c) the luminescence intensity of complex **5** in different concentrations of $Fe(NO_3)_3$ ethanol solutions, (inset) the dose-response graph at 543 nm revealing the Stern−Volmer quenching constant $K_{SV}$ was 0.0021 $\mu M^{-1}$ ($r^2$=0.990). ($\lambda_{ex}$ = 329 nm)

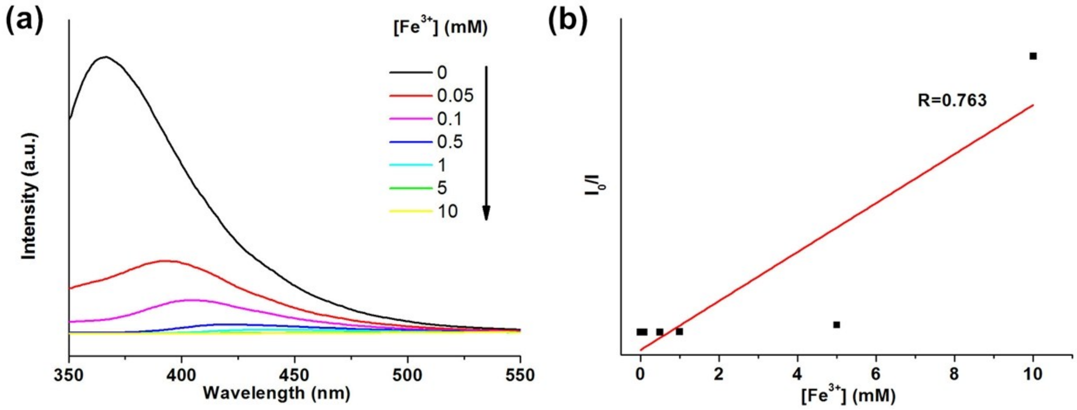

**Figure S7.** (a) The luminescence intensity of $H_2L$ upon addition of different concentrations of $Fe(NO_3)_3$ ethanol solutions; (b) the dose-response graph at 367 nm revealing the luminescence quenching of $H_2L$ by $Fe^{3+}$.

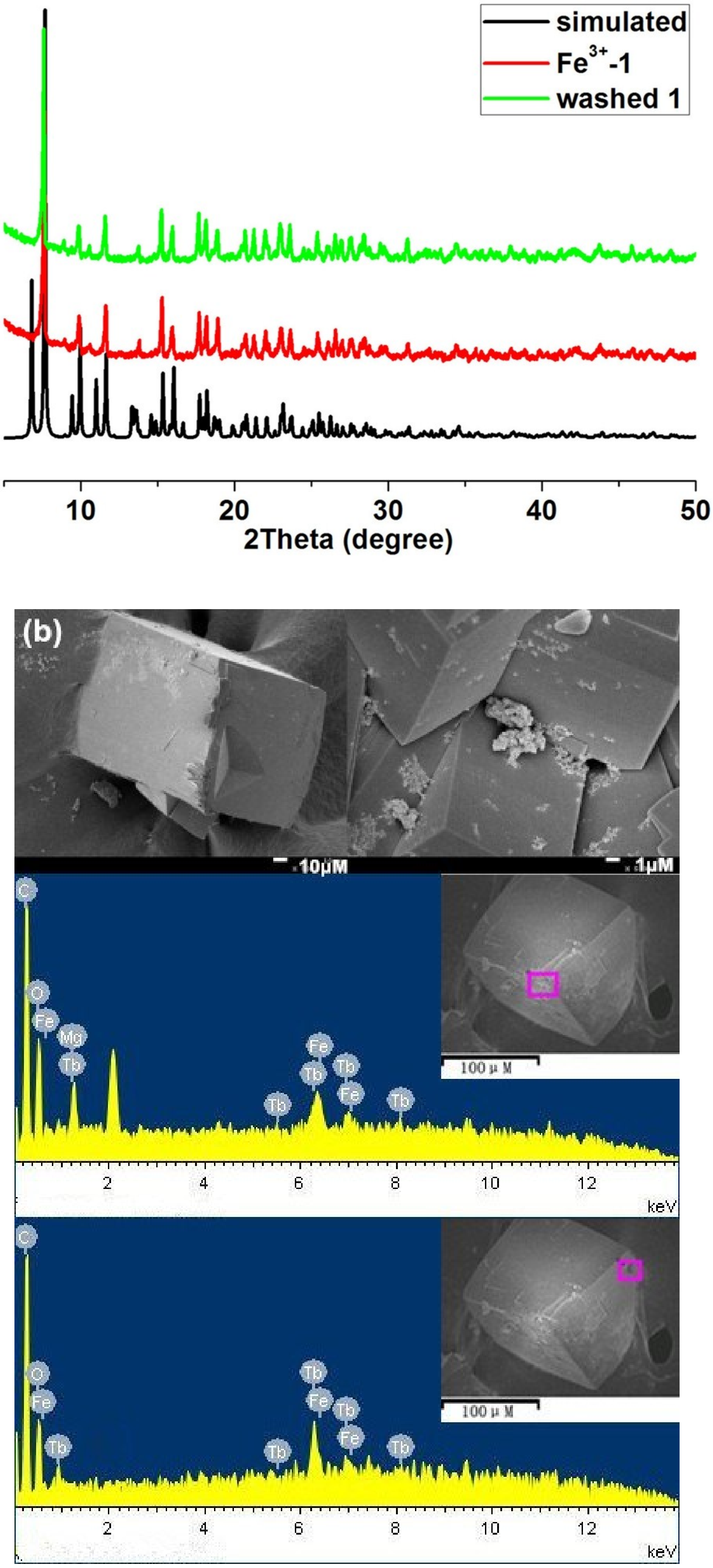

**Figure S8.** (a) The PXRD of Fe$^{3+}$-**1** and washed **1**; (b) the SEM and EDS of Fe$^{3+}$-**1**.

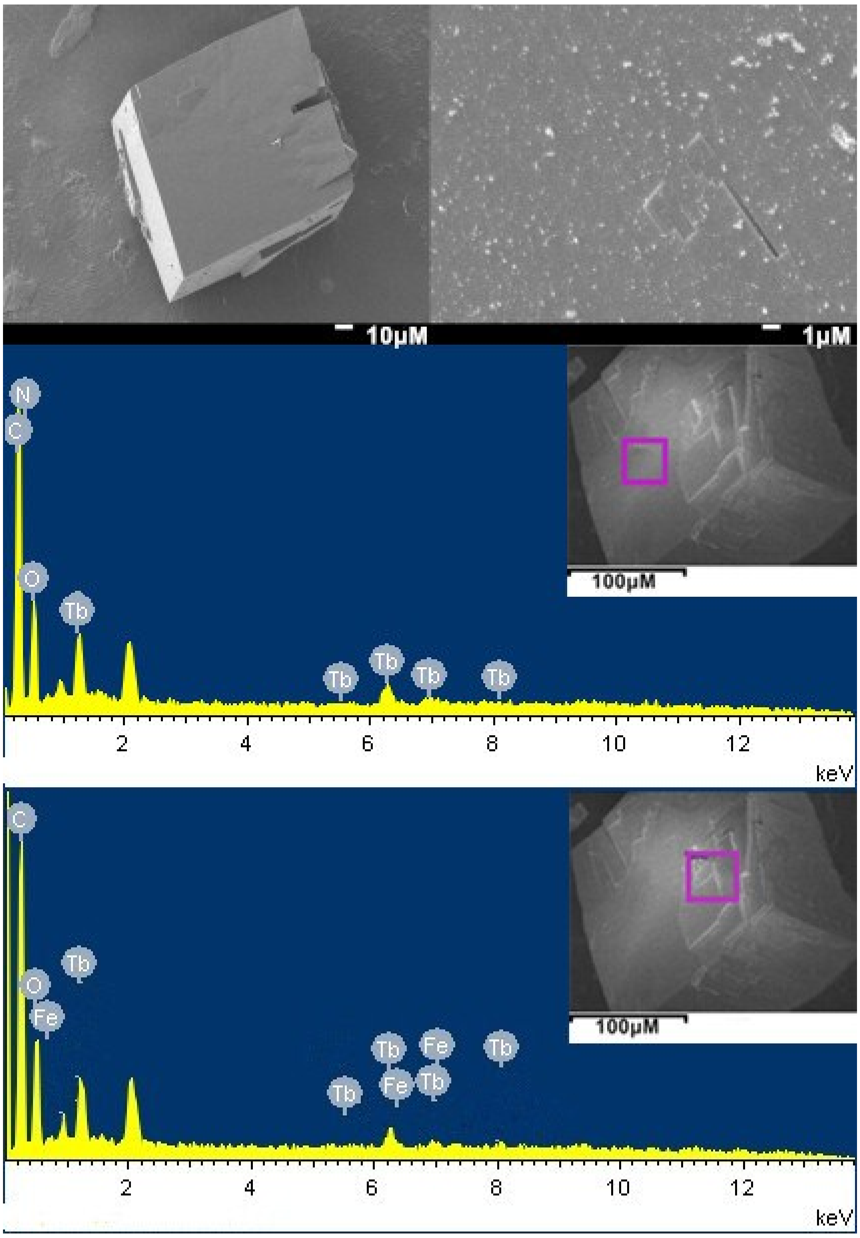

**Figure S9.** The SEM and EDS of washed **1**.

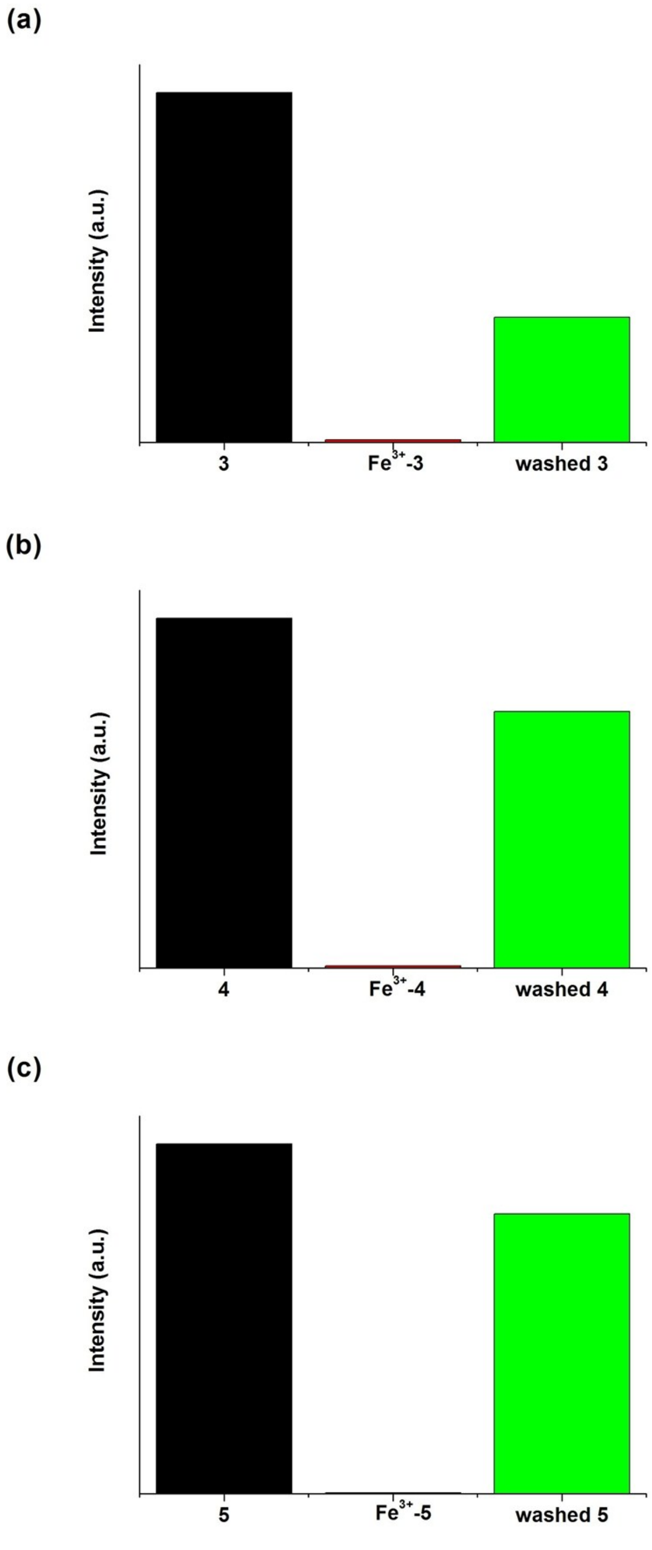

**Figure S10.** (a) The luminescence intensity of complex **3** at 619 nm in one cycle (after the washing, it was reverted to 35% of the initial state); (b) the luminescence intensity of complex **4** at 543 nm in one cycle (after the washing, it was reverted to 73% of the initial state); (c) the luminescence intensity of complex **5** at 543 nm in one cycle (after the washing, it was reverted to 80% of the initial state). ($\lambda_{ex}$ = 329 nm)

**Table S3**. The recovery efficiency of three recycles for **1**, **4**, **5** ($\lambda_{em}$ = 543 nm) and **3** ($\lambda_{em}$ = 619 nm).

| No. \ recovery efficiency (%) | a | b | c |
|---|---|---|---|
| 1 | 62 | 46 | 11 |
| 3 | 37 | 31 | 20 |
| 4 | 71 | 46 | 16 |
| 5 | 78 | 64 | 18 |

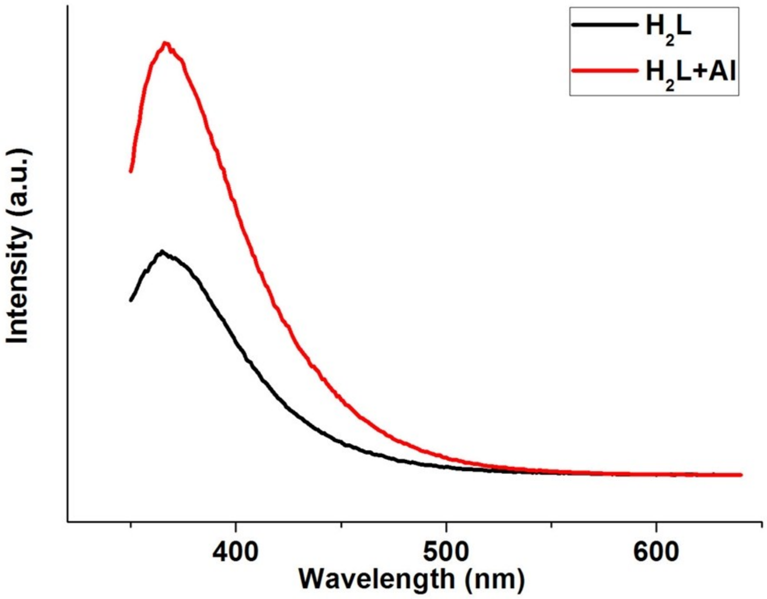

**Figure S11.** The luminescent of $H_2L$ in 3 mL 1 × $10^{-2}$ mol/L $Al^{3+}$ of ethanol solution ($\lambda_{ex}$ = 329 nm).

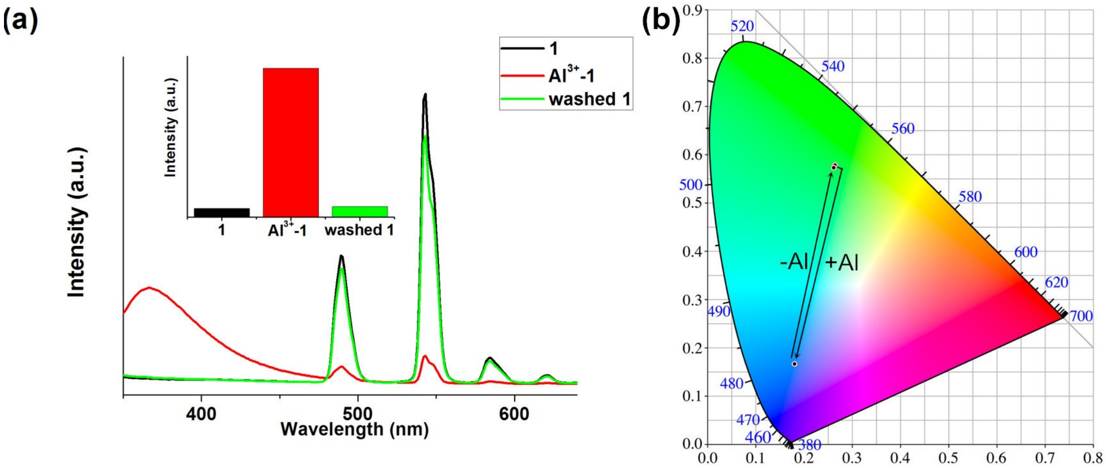

**Figure S12.** (a) The luminescent of complex **1** in an ethanol solution of 1×$10^{-2}$ mol/L $Al^{3+}$, (inset) the luminescent intensity of the ligand emission peaks at 365 nm ($\lambda_{ex}$ = 329 nm); (b) the corresponding CIE chromaticity coordinate.

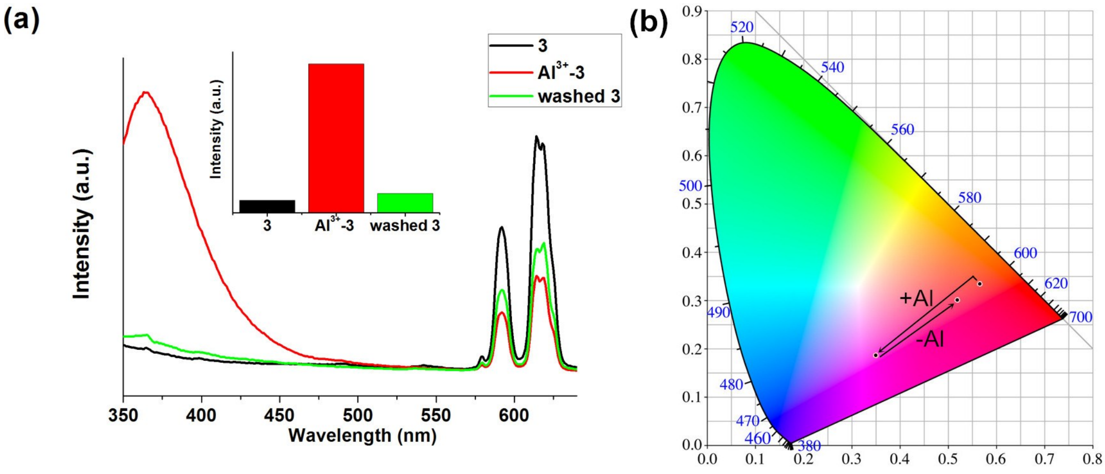

**Figure S13.** (a) The luminescent of complex **3** in an ethanol solution of 1 × $10^{-2}$ mol/L $Al^{3+}$, (inset) the luminescent intensity of the ligand emission peaks at 365 nm, and the emission at 619 nm can renew 57% of the initial state ($\lambda_{ex}$ = 329 nm); (b) the corresponding CIE chromaticity coordinate.

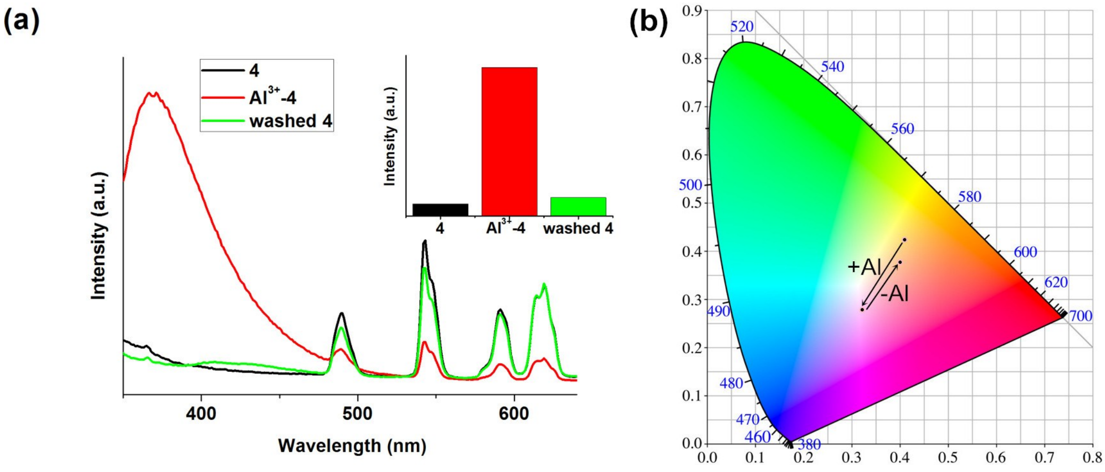

**Figure S14.** (a) The luminescent of complex **4** in an ethanol solution of 1 × $10^{-2}$ mol/L $Al^{3+}$, (inset) the luminescent intensity of the ligand emission peaks at 365 nm and the emission at 543 nm can renew 80% of the initial state ($\lambda_{ex}$ = 329 nm); (b) the corresponding CIE chromaticity coordinate (0.3218, 0.2789).

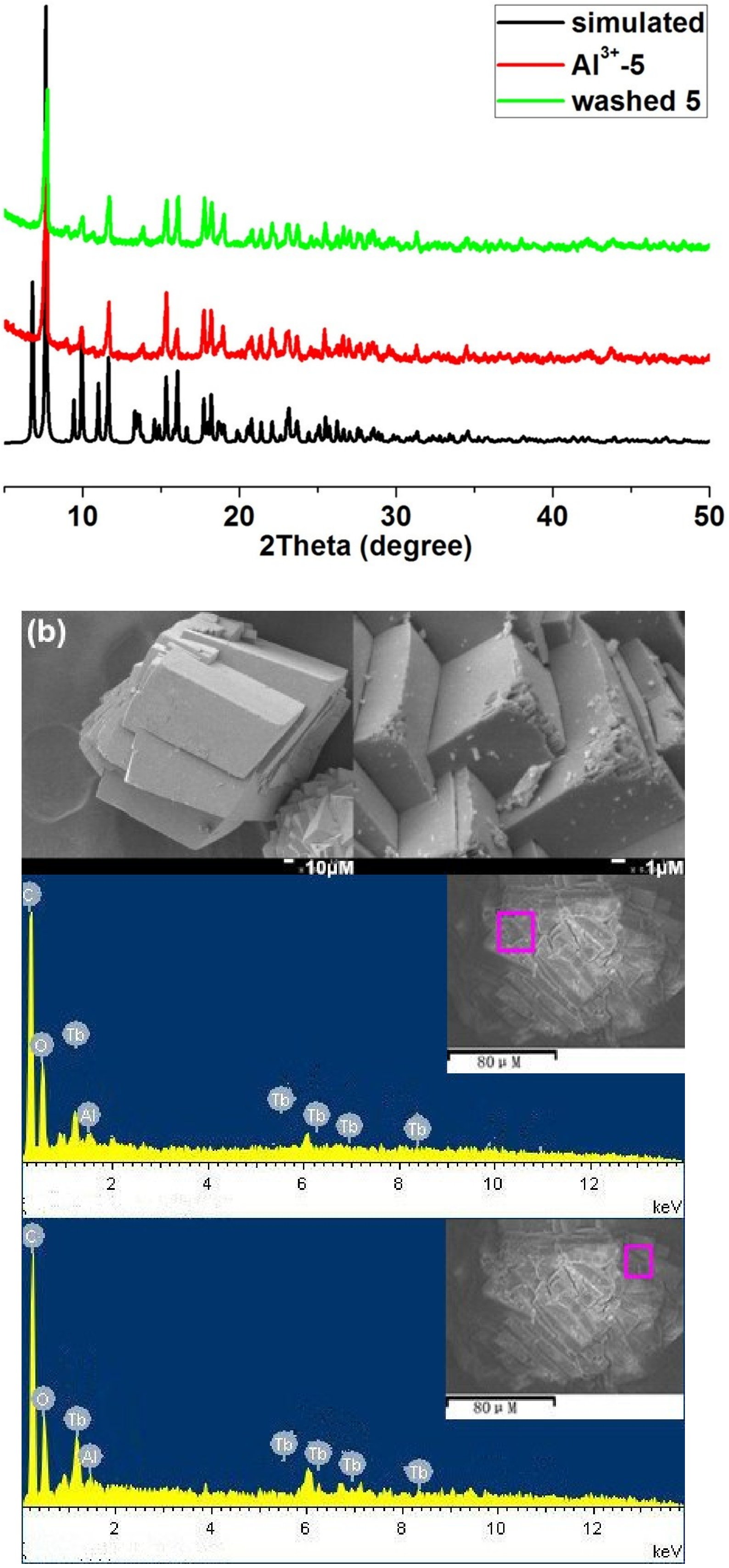

**Figure S15.** (a) The PXRD of Al$^{3+}$-**5** and washed **5**; (b) the SEM and EDS for Al$^{3+}$-**5**.

**Table S4**. The recovery efficiency of three recycles for **1**, **4**, **5** ($\lambda_{em}$ = 543 nm) and **3** ($\lambda_{em}$ = 619 nm).

| No. \ recovery efficiency (%) | a | b | c |
|---|---|---|---|
| 1 | 87 | 63 | 30 |
| 3 | 59 | 37 | 30 |
| 4 | 82 | 55 | 33 |
| 5 | 90 | 60 | 35 |

## Reference

1 Platon Program: A. L. Spek, Acta Crystallogr., Sect. A **1990**, 46, 194.